SLEEPER END RESISTANCE OF BALLASTED RAILWAY TRACKS

Louis Le Pen[1], PhD CEng MICE, Athma Ram Bhandari[2], PhD & William Powrie[3], FREng MA MSc PhD CEng FICE

[1]Research Fellow, University of Southampton, England, UK. email llp@soton.ac.uk

[2]Postdoctoral Fellow, Bureau of Economic Geology, The University of Texas at Austin, TX 78713, USA, email: athma.bhandari@beg.utexas.edu

[3]Professor of Geotechnical Engineering and Dean of the Faculty of Engineering and the Environment, University of Southampton, England, UK. email wp@soton.ac.uk

ABSTRACT

This paper describes model tests carried out to investigate the contribution to the resistance to the lateral movement of a railway sleeper attributable to the ballast shoulder, for a range of shoulder widths and heights. During the tests, the deflection and resistance were measured and photographs taken. Photographs were analyzed using a digital image correlation technique to identify the zones of ballast surface disturbance, these demonstrate that a bulbed failure volume is mobilized at the ultimate limit state. An idealised three dimensional failure mechanism is proposed and resistances are calculated using the limit equilibrium approach. The calculation is found to provide a reliable estimate of the measured resistance. The work identifies the optimum shoulder width and height. The calculations are extended to demonstrate that when a number of sleepers are moved simultaneously the sleeper end resistance may be 1/3 less per sleeper than that indicated in tests on an isolated sleeper. The image analysis and limit equilibrium calculations show that this is due to the overlapping of mobilized failure volumes from adjacent sleepers.

Keywords: Ballast, sleeper, shoulder, lateral resistance, model tests, scaled ballast, image analysis, limit equilibrium, railtrack, stability, digital image correlation

Introduction

Railway tracks must resist the lateral loads exerted by trains as a result of curving, wind loading and vehicle dynamic effects. Resistance to lateral forces is also required in the absence of train loading to prevent rail buckling as a result of temperature-induced self-stresses within the rails. In conventional ballasted railway track, lateral loads are transferred from the rails through the fastenings to the sleepers, and thence into the ballast. There are three components of lateral resistance, with different characteristics, associated with the three interfaces between the ballast and sleeper, at the sleeper base, in the crib (between adjacent sleepers), and in the shoulder (at the sleeper end). The resistance from the ballast shoulder depends on the shoulder size. The sleeper end resistance may be increased by extending either or both of the shoulder width $\boldsymbol{x}$ and the height $\boldsymbol{y}$ to which it rises above the top of the sleeper (Figure 1).

There has been some discussion in the literature concerning the relative importance of these three components of lateral resistance (Shenton and Powell 1973; ORE, 1976; Selig and Waters 1994), and the relative merits of increasing the ballast shoulder width and height (Kabo 2006). Laboratory lateral pull tests on a single sleeper by Le Pen and Powrie (2011) indicated relative contributions of base, crib and shoulder resistance of 26-35%, 37-50% and 15-37% respectively for a typical sleeper type and spacing for newly laid unloaded track (G44 sleepers at 0.65 m centers) and a range of shoulder sizes. This picture is more complex than the equal (33% each) contributions often suggested (e.g. ORE 1976). Furthermore the assumed equal split of base, crib and shoulder lateral resistance contributions is for unloaded track and does not explicitly recognize that the sleeper base resistance increases in proportion to train load, and therefore makes the most important contribution when the track is loaded. The crib and shoulder resistances do not increase with train loading; thus their contribution is critical to the prevention of temperature induced buckling of unloaded track.

The objectives of this paper are to

investigate the relative importance of the shoulder width x, and heap height y on the lateral resistance by means of model tests.

determine the zone of shoulder ballast disturbance using digital image analysis.

identify the failure mechanism and propose a representative failure wedge for further analysis.

quantify and compare the resistance for a given sleeper spacing and shoulder geometry by limit equilibrium calculation.

identify the optimum shoulder width and height.

Materials and procedure

Scaled ballast

Tests were carried out using a 1/3 scale ballast sourced from Cliffe Hill Quarry in Leicestershire, which also supplies Network Rail (NR) with full size ballast from the same parent rock (granite) having a specific gravity ($\boldsymbol{G_s}$) of 2.78. The particles were mapped to a 1/3 scale parallel gradation as indicated in Figure 2, using the nearest available ASTM sieve sizes.

Full size ballast was also obtained and a detailed comparison using image analysis of the shapes of particles in sieve intervals ranging from scaled to full size ballast was carried out. This study is reported fully in Le Pen et al., (2013) where the results demonstrate that over the relatively small scaling factor (1/3) used the form and roundness of the particles changed only slightly, in broad agreement with the findings of Sevi (2008). To illustrate how similar the particles are across the size range Figure 3 shows plan view images of randomly selected ballast particles from scaled to full size. The images have been scaled so that the particles appear the same size; no difference in shape associated with the difference in particle size is discernible with the naked eye.

Monotonic triaxial tests on the scaled ballast (Aingaran, 2013) on dry samples 150 mm diameter × 300 mm in height using commercially available apparatus (GDS, 2013) were carried out to determine the effective angles of shearing resistance over a range of confining pressures (Table 1). The triaxial tests were carried out from an average initial dry density of 1560 kg/m^3 which is towards the upper middle of the dry density (γ_d) range achievable in laboratory compaction tests (1391 kg/m^3 to 1623 kg/m^3). Figure 4 compares the peak angles of effective shearing resistance for the scaled ballast with data taken from the literature for tests on full size samples over a range of initial confining pressures. Further details of the tests from the literature are summarised in Table 2. The full size tests comprise six test series on ballast materials of similar gradations of mainly igneous (granite, basalt, dolomite) rock types, with one sedimentary rock type (limestone). The dotted line in Figure 4 shows the general trend for membrane-corrected results on scaled ballast. Figure 4 illustrates that the effective strength of the scaled ballast generally falls within the range of values for different full size ballasts, and is perhaps at the lower end of that range for confining stresses between 10 kPa and 30 kPa.

The confining stress within a ballast shoulder is likely to be 10.0 kPa or less at full scale. However, it is extremely difficult to carry out reliable triaxial tests on rockfills and ballasts at such low confining stresses, owing to the tendency of specimens to collapse under their own weight. The scaled ballast specimens tested in support of the research presented in this paper were encased in 2 mm thick latex membranes having a neutral stress internal diameter of 150 mm. Suction was applied to permit removal of the split mould; if this suction fell much below 15 kPa, the specimen would barrel and/or collapse prior to testing. Even if outright failure does not occur, barrelling can induce significant membrane confinement stresses. Therefore no tests were carried out on the scaled ballast at a confining stress of less than 15 kPa. Similarly, there are very few tests on rockfills/ballasts reported in the literature carried out at a confining stress of less than 10 kPa. In such tests as are reported, it is generally unclear how membrane effects have been allowed for. Thus tests carried out at confining stresses of less than 10 kPa have been excluded from consideration in this paper.

Leps (1970) collected data from a number of triaxial tests on rockfills carried out over the previous 40 years. Plotting the peak angle of effective shearing resistance against the logarithm of the effective confining stress demonstrated an approximately linear relationship, with the effective angle of shearing resistance being greater at lower confining stresses. The tests reported by Leps (1970) were carried out at confining stresses between 50 kPa and 3500 kPa. Extrapolation beyond this range of confining stress is unreliable, as the effective angle of shearing resistance cannot increase or decrease indefinitely even on a logarithmic scale. It also seems probable that none of the test data reported by Leps (1970) were corrected for membrane effects; it is now recognized that unless such a correction is made, angles of shearing resistance at low confining stresses will be substantially overestimated.

Fukushima et al. (1984) investigated the influence of membrane correction on data from tests on sand at low confining stresses. They demonstrated that when membrane effects are corrected for, the angle of effective shearing resistance does not increase indefinitely with decreasing confining stress but plateaus (i.e., it reaches a peak value that does not increase further) at a confining stress of approximately 50 kPa.

To illustrate the importance of membrane correction, Figure 4 also shows both the uncorrected and corrected data for the tests on scaled ballast. Membrane effects were corrected using the hoop stress method described by Fukushima et al. (1984) and Henkel and

Gilbert, (1952). This method is appropriate for drained samples where the membrane is liable to buckle. Applying this correction reduced the peak angle of effective shearing resistance at a cell pressure of 15 kPa by approximately 2º for the 2 mm thick latex membranes used. The difference between corrected and uncorrected values would be more significant for thicker and/or stiffer membranes. Figure 4 shows that the corrected angles of shearing resistance for the scaled ballast plateau at approximately 48º at a cell pressure of approximately 60 kPa, while the effect of the membrane is negligible at confining stresses in excess of 100 kPa.

In summary:

The shape (form and roundness) of the ballast used in this study changes only slightly over the scaling range.

The scaled ballast has an effective angle of shearing resistance comparable with a variety of full size ballasts.

In the literature there is a large range of reported angles of shearing resistance for ballasts particularly at low confining stresses. However, this seems to result from a failure to correct consistently for membrane effects, which is essential at lower confining stresses.

On the basis of the results presented in Figure 4 and the review of the literature summarized above, this investigation will consider a range of peak angles of shearing resistance from 45º to 55° for the model tests, for which the range of confining stress is likely to be 0 to 4 kPa. Although these tests use scaled material and are presented as models, they nonetheless represent real events that can be examined in their own right to give insights into the geometry of the failure mechanisms that occur.

Experimental set-up and test details

The experiment modelled a 1/3 size sleeper end being pushed gradually into a shoulder formed of scaled ballast. Displacements were monitored by LVDT and optically and the resistance on the sleeper end by means of a load cell.

The model ballast shoulder was confined between vertical wooden borders located well beyond the expected extent of the failure mechanism (which varied according to the shoulder size), as indicated in the plan view of the test set-up shown in Figure 5. The boundaries of the testing apparatus could therefore have had no influence on the results. The ballast bed extended to a depth of 110 mm below the bottom of the model sleeper end, corresponding to 330 mm at full scale. A rough sandpaper mat at the base of the ballast prevented ballast particles from sliding along the interface with the wooden surface on which the tests were carried out.

The scaled sleeper end was based on a 1/3-size G44 sleeper with slightly simplified geometry. The full scale sleeper end is a trapezium of base width 0.285 m, height 0.210 m and top width 0.200 m. The scaled sleeper end was a rectangle of 0.285/3 = 0.095 m width and 0.2/3 = 0.067m height. However, the exact geometry of the model sleeper is unimportant, as long as it is known. A wide range of sleepers is in use worldwide, and while their cross-sections vary in shape all correspond approximately (and in the case of all wooden and plastic sleepers and many concrete sleepers exactly) to a rectangle.

The volume of ballast mobilized in the failure mechanism is expected to be $1/3^3$ or 1/27 of the full scale volume hence the sleeper end resistance should be 1/27 of that at full scale. All data reported in this paper are given as at full size, i.e. with displacements measured in the model multiplied by 3 and resistances (which are primarily from the weight of the wedge) are multiplied by 27. Scaling laws are discussed by Powrie, (2004).

Following placement of the ballast in the desired geometry, the model sleeper end was pushed slowly into the shoulder by means of a screw jack acting via a ram onto the load cell. Unrealistic upward movement of the sleeper end was prevented. Table 3 summarizes the test geometries investigated; the dimensions given are defined in Figure 1 and Figure 5.

The slope angle beyond the shoulder crest was approximately 45º, which was achieved naturally by the ballast as it was placed.

Image acquisition and analysis

Images of the ballast surface were taken from above using a 10 megapixel digital camera for observing and measuring ballast movement during the tests. The image scales were approximately 4.9 pixels per mm (for the 500 mm wide testing area, Figure 5a) and 3.5 pixels per mm (for the 1000 mm wide testing area, Figure 5b).

The captured images were analyzed incrementally using the digital image correlation technique described by Bhandari et al. (2012). The technique involves defining measurement (tracking) points and identifying corresponding patterns at these points in the subsequent images using a normalized cross-correlation algorithm. The basic assumptions are that the pattern is approximately constant between successive images and that the local textural information is unique. The natural variation of texture in ballast particles was found to be sufficient for this purpose. Measurement points at a grid spacing of 70 pixels and image subsets of 65 × 65 pixels (approx. 13.3 mm x 13.3 mm for an image resolution of 4.9 pixels/mm and 18.6 mm x 18.6 mm for an image resolution of 3.5 pixels/mm) were used. The technique does not track individual ballast particles or rotations but is capable of providing a clear picture of overall movements.

Resistance- displacement and image analysis results

Resistance-displacement plots

Figure 6 and Figure 7 show the measured sleeper end resistance as a function of displacement for all of the shoulder geometries tested. Tests were repeated under the same shoulder geometry to assess the repeatability of the measurements.

From Figure 6 two phases of behavior are apparent with increasing shoulder width $\boldsymbol{x}$ and zero shoulder heap height $\boldsymbol{y}$:

Initially as the shoulder width ($\boldsymbol{x}$) is increased, both the peak resistance and the deflection at which it is fully mobilized increase.

Beyond a certain threshold shoulder width ($\boldsymbol{x}$ between 600 mm and 800 mm for a shoulder heap height $\boldsymbol{y} = 0$), the peak resistance and the deflection at which it occurs remain constant.

This is consistent with there being no benefit in terms of an increased resistance in extending the shoulder beyond the point where the failure surface daylights. Raising the height of the ballast shoulder above the level of the sleeper top (Figure 7) increases the threshold shoulder width, although in the tests with an equivalent 125 mm heap of ballast y the threshold has not been reached.

In tests on real track, the peak lateral resistance in pull out tests has been reported to occur usually within 20 mm of sleeper movement (ERRI committee D202 report 2, 1995). However, this is for the combined effects of crib, base and shoulder ballast on generally well trafficked track. Beneath the sleeper, traffic loading densifies the ballast whereas the shoulder ballast is likely to remain at its as-placed density. The model tests were therefore carried out on just-placed shoulder ballast. They indicate that the peak resistance from the shoulder alone occurs at displacements generally between 20 mm and 40 mm, but up to 60 mm in one case.

Table 4 shows average values of peak shoulder resistance and corresponding displacements from the model tests, with the results again given as at full size.

Image analysis results

Figures 8 to 14 show the image analysis results presented as displacement vector plots and contours of displacement magnitude at a sleeper end displacement close to the mobilization of peak resistance (Table 4). However, in some tests the contour plots are produced for smaller sleeper end displacements (Tests A and E) because the image analysis was compromised at larger displacements due to the ballast falling downslope. Also indicated is the centerline of the crib ballast for a sleeper spacing of 0.65 m, the ballast shoulder slope crest and a plan view of an idealized failure wedge mechanism (explained in section 4). The displacement contours are shown at 5%, 10%, 15%, 20% and 25% of the sleeper end movement. These values were chosen to highlight the overall shape of disturbance. Arrows show the displacement vectors with their size in proportion to the movement. The caption for each figure gives the sleeper end movement. The contour furthest from the sleeper is the 5% contour with the displacement generally increasing with proximity to the sleeper. The actual displacement represented by each contour is then determined by multiplying the percentage by the sleeper end movement shown in the caption.

Figures 8 to 14 indicate that the zone of disturbed material as viewed in plan is bulb-shaped and in all cases extends into the region of shoulder ballast closer to the adjacent sleepers at 0.65 m spacing.

Failure wedge approximation of the observed failure mechanism

Le Pen and Powrie (2011) proposed a failure mechanism for estimating the resistance provided by a ballast shoulder of a given width x, height y above the sleeper top, and effective angle of shearing resistance ϕ' (Figure 15). The mechanism involves a wedge of ballast defined by one near-horizontal and two vertical failure planes being moved relative to the rest of the shoulder by the sleeper end (Figure 15b and 15c). Analysis using this mechanism gave results reasonably consistent with full size tests by Le Pen and Powrie (2011) on a full scale section of track in the laboratory one sleeper bay wide. However, there was a wide range of uncertainty in these tests in evaluating the contribution to measured

lateral resistance of the crib and shoulder, owing to the difficulty in subtracting out the contribution of the base, which appeared to be the most variable component of measured resistance. It was also recognized that the boundaries of the testing apparatus may have influenced the results. These problems have been overcome in the model tests reported in this paper and a comparison of the measured and calculated resistances for the ballast shoulder alone as well as an assessment of the validity of the failure mechanisms assumed is now possible.

Limit equilibrium methods are well established for long geotechnical constructions such as embankment and cutting slopes and retaining walls, which are analyzed in plane strain. However, the width of a railway sleeper is not large in relation to its other dimensions, and the failure surfaces at the sleeper end will spread out to form a three-dimensional mechanism. This introduces more additional unknown (out-of-plane) forces than equilibrium equations, making the problem statically indeterminate. Le Pen and Powrie (2011) dealt with the statical indeterminacy of the problem by making a number of simplifying assumptions, as explained below.

There are three unknown forces acting on the failure wedge (i.e. the reactions $\boldsymbol{R'_w}$, $\boldsymbol{R'_b}$ and $\boldsymbol{R'_s}$ at the interface with the sleeper end, and the ballast at the base sides respectively). In the general case the wedge splay angle $\boldsymbol{\alpha}$ (viewed in plan, Figure 15b) is unknown; and because the equation of horizontal equilibrium along the line of the track is automatically satisfied by symmetry, $\boldsymbol{R'_s}$ cannot be determined. However, if it is assumed that $\boldsymbol{\alpha}$ is equal to $\boldsymbol{\phi'}$, the resultant force on the vertical shear planes acts in the longitudinal horizontal direction and $\boldsymbol{R'_s}$ disappears from the equation of lateral horizontal equilibrium. The vertical component of the interface reactions on the wedge sides is neglected, but this is reasonable if the main sliding plane is near-horizontal. The mechanism can then be defined in terms of a single variable (the angle $\boldsymbol{\theta_w}$) and the fixed geometry and strength parameters $\boldsymbol{\delta}$ and $\boldsymbol{\phi}$). The weight $\boldsymbol{W}$ of the soil involved in the failure mechanism can be determined, and the remaining unknowns $\boldsymbol{R'_b}$ and $\boldsymbol{R'_w}$, and hence the horizontal component of $\boldsymbol{R'_w}$, found.

This simplified approach can be modified to consider the interaction of failure zones between adjacent sleepers that are spaced more closely than the width of ballast displaced, by subtracting out the contribution from the overlapping volumes of ballast (thus modifying $\boldsymbol{W}$) for a range of wedge angles and finding the minimum shoulder resistance as before.

The failure wedge shown in Figure 15 was used in analysis to estimate the theoretical lateral sliding resistance offered by ballast shoulders of different geometry adjacent to a single sleeper on full size track. The parameters used in the analysis are shown in Table 5; these are the same as those used by Le Pen and Powrie (2011).

The calculations have been carried out for effective angles of shearing resistance of 45º, 50º and 55º for the ballast which is intended to cover the range of possible values of peak angle of effective shearing resistance in the as placed shoulder ballast based on the triaxial test results discussed in the section Materials and Procedures.

Limit equilibrium failure shape and comparison to displacement fields

Table 6 shows the positions (viewed in plan) at which the corners of the theoretical critical failure wedge daylight, relative to the midpoint of the sleeper end (dimensions x_f and z_f with the subscript f to denote failure), together with the critical failure wedge angle θ_w (Figure 15). These data may be compared with the zones of disturbance identified by image analysis at sleeper end displacements corresponding to the mobilization of the peak resistance. To aid this comparison the daylight positions of the failure wedges calculated using a 50º angle of effective shearing resistance for the ballast were shown by thick black lines in Figures 8 to 14.

Reviewing Figures 8 to 14 it can be seen that while the side splay angles nearest to the sleeper end are reasonably close to those assumed in the idealized mechanism, the calculated daylight positions of the corners of the wedge are well beyond the limits of the measured zone of disturbance. This apparent discrepancy could be a result of the ability of the ballast to dilate and move upward at the very low effective stresses near the surface. It could also be due to a sleeper width to particle size ratio effect: the curvature of the disturbed zones away from the idealized failure lines apparent in the figures was not seen in initial tests using the same model sleeper end pushed into Leighton Buzzard sand.

In any case, the discrepancy occurs at the shallowest point of the mechanism: hence in volume terms is slight. For example, in Figure 8 the observed movement does not extend to the far corners of the calculated failure mechanism. However, the depth and weight of material near to the far corners is small and contributes only a small proportion of the calculated resistance. Although the image analysis suggests that for wide shoulders the disturbed zone may extend further out from the sleeper than the idealised mechanism would indicate, this is probably an artifact of ballast falling from the crest, rather than being actively involved in the failure wedge resisting the load.

Comparison of measured and calculated resistance

Experimental data from lateral pull tests on unloaded track (Office for Rail Research and Experiments of the International Union of Railways, ORE, 1976) were used by the European Rail Research Institute (ERRI committee D202 report 2, 1995) to develop a graph showing the increase in resistance (y-axis) for level and heaped shoulders of increasing width (x-axis), expressed as a % above that when no shoulder is present. Le Pen and Powrie (2011) converted the ERRI results from this proportional form to an estimate of the absolute magnitude of shoulder resistance, and concluded that their own tests (carried out on a single sleeper bay within a laboratory) were in reasonable agreement with the data used by ERRI.

Figure 16 compares the ERRI data (as interpreted by Le Pen and Powrie 2011) with the results from the model tests using scaled ballast and limit equilibrium calculations for ballast shoulders of increasing width with no heap above the sleeper top. The ERRI data do not extend beyond a shoulder of lateral width 0.6 m.

Figure 17 shows the same information for tests in which the ballast shoulder was heaped to 125 mm above the sleeper end top.

322 Figures 16 and 17 demonstrate that the measured peak resistances in the physical tests closely
323 match the calculated results for a soil with an angle of effective shearing resistance of
324 approximately 50º. This is a key finding, as it suggests that despite the approximations and
325 simplifications adopted, the sleeper end failure mechanism analysis proposed by Le Pen and
326 Powrie (2011) can give a reasonable indication of the benefit of a ballast shoulder of a given
327 size and shape.

328 Figures 18 and 19 show the limit equilibrium calculated resistance per sleeper for a 0.65 m
329 sleeper spacing (as used on many mainline railways), taking into account the reduction due to
330 the overlapping of the mechanisms associated with adjacent sleepers (i.e. by subtracting the
331 mass of the overlapping volume used to determine the weight term $\boldsymbol{W}$ in Figure 15 of the
332 limit equilibrium calculation).

333 Comparison of Figures 16 and 17 with Figures 18 and 19 shows that taking account of the
334 effect of overlapping failure wedges gives a significantly reduced shoulder resistance per
335 sleeper when the sleeper spacing is 0.65 m. For an effective angle of shearing resistance of
336 50º, the reduction is at least 1/3 for lateral shoulder widths ($\boldsymbol{x}$) greater than 0.3 m. This is
337 important because rail buckles typically occur over a length covering several sleeper ends, so
338 the reduced resistance per sleeper spacing is a more realistic estimate of the resistance
339 available to prevent buckling than that obtained from testing a single sleeper in isolation.

340 It is also worth noting that as the sleeper spacing reduces these calculations tend to a plane
341 strain calculation and with the typical sleeper dimensions and spacing in the UK the resulting
342 force magnitudes calculated are only slightly less than that predicted from a traditional plane
343 strain approach.

344 The results can also be considered in terms of volume efficiency, i.e. the volume of the
345 ballast shoulder above the level of the sleeper base needed to provide a unit of resistance.
346 Results for an angle of effective shearing resistance of 50º are shown in Figure 20 for both an
347 isolated sleeper and per sleeper at 0.65 m spacing. This shows that, as the shoulder is
348 extended, it continues to become more efficient as well as providing an increasing lateral
349 resistance, until the shoulder extends to the distance at which the failure surface daylights.
350 Further increases in shoulder width provide no additional lateral resistance, and result in
351 decreasing volume efficiency.

352 Figure 20 also indicates that a given volume of ballast will increase the lateral resistance
353 more efficiently if it is used to increase the shoulder width rather than the heap height, up to
354 the point at which the threshold width is reached. Beyond this, there is no benefit in
355 extending the shoulder but an increase in resistance can still be obtained by using additional
356 material to raise the heap height.

357 Conclusions and Implications for practice

358 Both model tests and limit equilibrium calculations have shown that the sleeper end
359 resistance increases with ballast shoulder width, up to a certain threshold value which
360 coincides with the position at which the failure surface daylights. There is no benefit in
361 extending the shoulder width beyond this threshold value, as the critical failure mechanism is
362 not affected and the peak resistance remains constant. The threshold value depends on the
363 shoulder heap height. For ballast having an effective angle of shearing resistance of 50º, the

limit equilibrium calculations show that the threshold width of a level shoulder is approximately 0.75 m, rising to about 0.85 m for a shoulder with a heap height of 125 mm.

The limit equilibrium calculation proposed by Le Pen and Powrie (2011), with an angle of effective shearing resistance of 50º, has been shown to provide a reasonable estimate of the sleeper end resistance measured in model tests. Consistency between the model tests and full scale tests reported in the literature has also been demonstrated.

The zones of disturbance identified in the image analysis are bulbed rather than defined by straight lines as assumed in the limit equilibrium analysis but the discrepancies are probably near-surface effects and there is reasonable agreement between the width of the disturbed zone away from the sleeper and more importantly the initial sideways spread or splay angle of the vertical boundaries to the failure wedge.

The effectiveness of a shoulder of given geometry can be expressed as a volume efficiency, i.e. the volume of material needed to give a unit of resisting force. The shoulder is at its most efficient at the threshold width. Until the threshold width is reached, a given volume of ballast added to a shoulder will be more effective as extra width than height. Once the threshold width has been reached, additional material should be used to create heap height, as further increases in shoulder width will not bring about any increase in sleeper end resistance.

Limit equilibrium calculations show that the resistance available per sleeper when account is taken of the overlapping of the failure mechanisms associated with adjacent sleepers is at least 1/3 less than for isolated sleepers. Owing to the close sleeper spacing and overlapping failure volumes this is only slightly different from the force in a traditional place strain calculation. This has implications for determining lateral resistance to track buckling on the basis of isolated sleeper pull tests.

Acknowledgements

The authors are grateful for the financial support of the Engineering and Physical Sciences Research Council (EPSRC). This work was made possible by combining techniques developed in two separate EPSRC grants: (1) “Development and role of structure in railway ballast”, EP/F062591/1 and (2) “Micro-Mechanical Behaviour of Locked Sands” GR/T22896/01. We also acknowledge and thank research students Sinthuja Aingaran and Sharif Ahmed for their contributions related to the development and use of scaled ballast.

References

Aingaran S., Forthcoming: 2013. Experimental investigation of static and cyclic behaviour of scaled railway ballast and the effect of stress reversal, Thesis. Faculty of Engineering and the Environment, University of Southampton, UK.

Anderson, W., and Fair, P. 2008. Behavior of railroad ballast under monotonic and cyclic loading. *J. .Geotech. .Geoenviron. Eng.*, 134(3), 316–327.

Aursudkij, B., McDowell, G. R., and Collop, A. C. 2009. Cyclic loading of railway ballast under triaxial conditions and in a railway test facility. *Granular Matter*, 11, 391–401.

Bhandari, A. R., Powrie, W., and Harkness, R. M. 2012. A digital image-based deformation measurement system for triaxial tests. *Geotech. Test. J.,* 35(2), 209–226.

ERRI. 1995. European Rail Research Institute, committee D202: Improved knowledge of forces in CWR track (including switches), Report 2, Review of existing experimental work in behaviour of CWR track. European Rail Research Institute, Arthur van Schendelstraat 754, NL – 3511 MK UTRECHT.

Fukushima, S., and Tatsuoka, F. 1984. Strength and deformation characteristics of saturated sand at extremely low pressures. *Soils Found.,* 24(4), 30–48.

GDS. 2013. *Geotechnical Digital Systems Intruments* [online]. Available: http://www.gdsinstruments.com/gds-products/triaxial-automated-system-load-frame-type [Accessed October 2013]

Henkel, D. J. & Gilbert, G. D. 1952. The effect of the rubber membrane on the measured triaxial compression strength of clay samples *Geotechnique*, 3, 20 to 29.

Indraratna, B., Ionescu, D. and Christie, H. 1998. Shear behavior of railway ballast based on large-scale triaxial tests. *J. Geotech. Geoenviron. Eng.*, 124(5), 439–450.

Kabo, E. 2006. A numerical study of the lateral ballast resistance in railway tracks. *Proc. Imech E. Journal of Rail and Rapid Transit,* 220, 425–433.

Le Pen, L., and Powrie, W. 2011. Contribution of base, crib, and shoulder ballast to the lateral sliding resistance of railway track: a geotechnical perspective. *Journal of Rail and Rapid Transit,* 225**,** 113–129.

Le Pen, L., Powrie, W., Zervos, A., Ahmed, S. & Aingaran, S. 2013. Dependence of shape on particle size for a crushed rock railway ballast. *Granular Matter*,doi: 10.1007/s10035-013-0437-5.

Leps, T. M. 1970. Review of shearing strength of rockfill. *Soil Mech. Found. Eng.,*96, 1159–1170.

Powrie, W. 2004. Soil Mechanics: Concepts and Applications, London, Spon.

ORE. 1976. A study of the factors influencing the resistance to transverse displacement of *unloaded track,* Office for Research and Experiments of the International Union of Railways, Commitee D 117 Report 8, October 1976.

RSSB. 2003. Rail Safety and Standards Board (RSSB) GC/RT5021: *Railway Group Standard: Track System Requirements*. Rail Safety and Standards Board, Evergreen House, 160 Euston Road, London, NW1 2DX.

Raymond, G. P., and Davies, J. R. 1978. Triaxial tests on Dolomite railroad ballast. *J. Geotech. Eng. Div.*, 104, 737–751.

436 Railtrack. 2000. Safety and Standards Directorate RT/CE/S/006 *Railtrack Line Specification:*
437 *Track Ballast and Stoneblower Aggregate*. Railtrack Plc, Railtrack House, Euston Square,
438 London, NW1 2EE.

439 Selig, E. T., and Waters, J. M. 1994. *Track Geotechnology and Substructure Management,*
440 London, Telford.

441 Sevi, A. F. 2008. Physical modeling of railroad ballast using the parallel gradation scaling
442 technique within the cyclical triaxial framework. PhD Thesis, Missouri University of Science
443 and Technology.

444 Shenton, M. J., and Powell, M. C. 1973. Draft report on British Rail lateral ballast resistance
445 tests, British Rail research sectional note 142 (unpublished).

446 Suiker, A. S. J., Selig, E. T., and Frenkel, R. 2005. Static and cyclic triaxial testing of ballast
447 and subballast. *J. Geotech. Geoenviron. Eng.*, 131(6), 771–782.

448

449 **FIGURES**

450

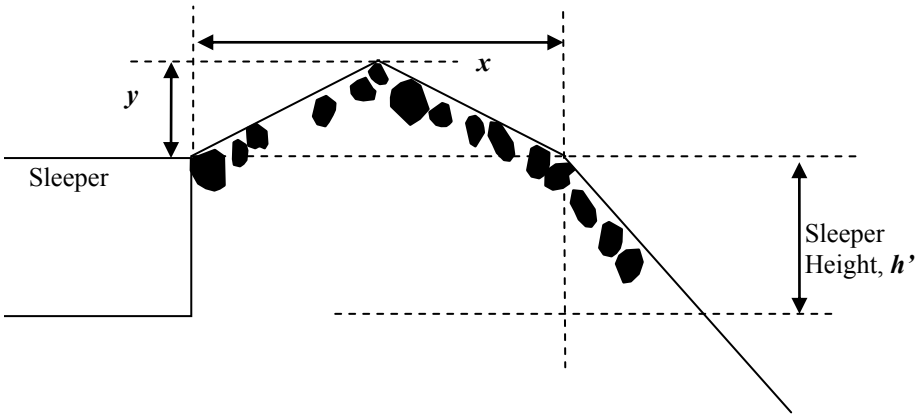

451

452 **Figure 1: Ballast shoulder**

453

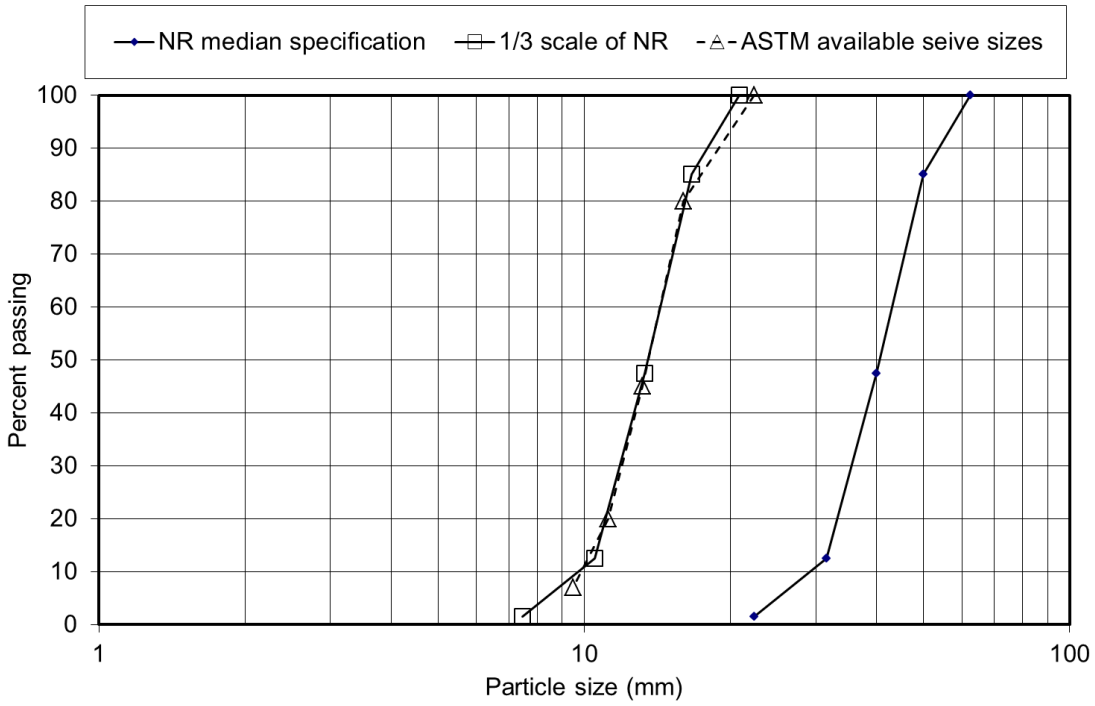

454

455 **Figure 2: Median ballast grading (Railtrack, 2000)**

456

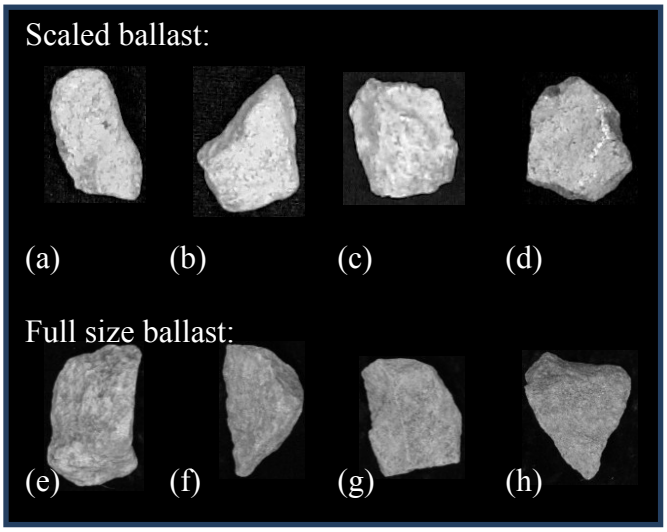

457

458 **Figure 3: Example particles in sieve intervals in mm: (a) 9.5 to 11.2 (b) 11.2 to 13.2 (c) 13.2 to 16.0, (d)**
459 **16.0 to 22.4 (e) 22.4 to 31.5 (f) 31.5 to 40.0 (g) 40.0 to 50.0 (h) 50.0 to 62.5**

460

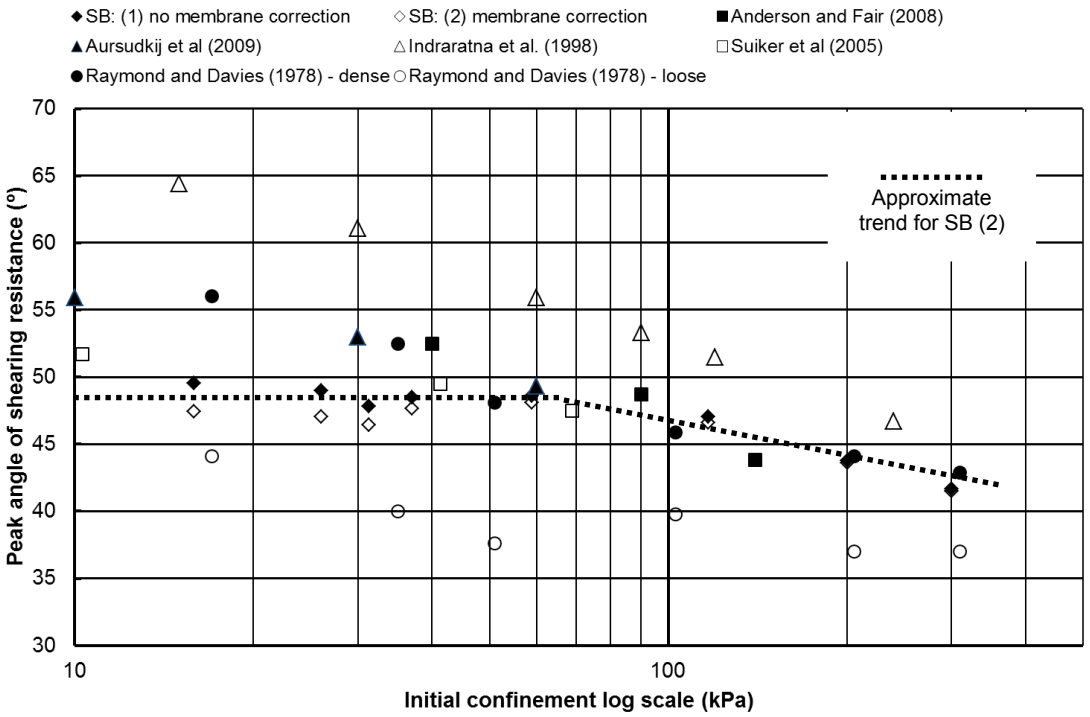

461

462 **Figure 4: Comparison of triaxial test data from tests on full size and scaled ballast (SB) and showing the**
463 **effect of membrane correction on the scaled ballast results.**

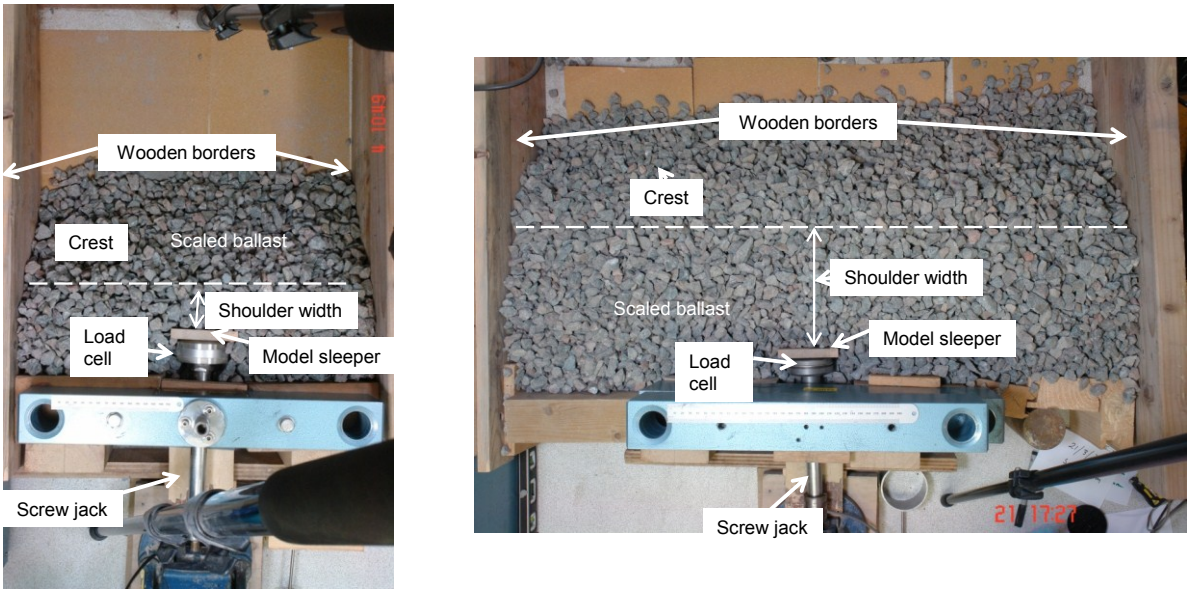

(a) Width of testing area = 500 mm

(b) Width of testing area = 1000 mm

464

465 **Figure 5: Plan view of experimental set-up used in scaled ballast tests to determine sleeper end resistance**

466

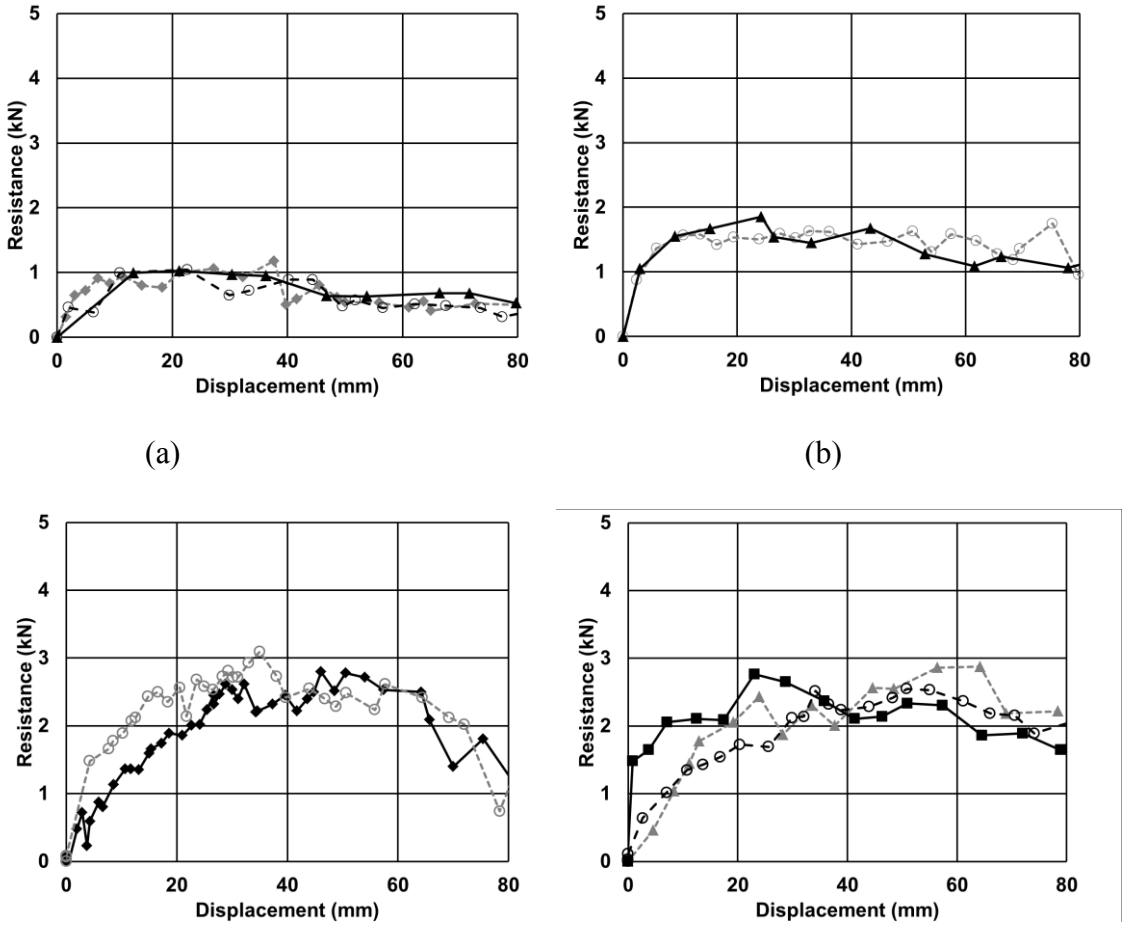

Figure 6: Sleeper end resistance versus displacement plots: (a) Test A: x = 200 mm, y = 0 mm (b) Test B: x = 400 mm, y = 0 mm (c) Test C: x = 600 mm, y = 0 (d) Test D:x = 800 mm, y = 0 mm (dimensions and loads as at full scale)

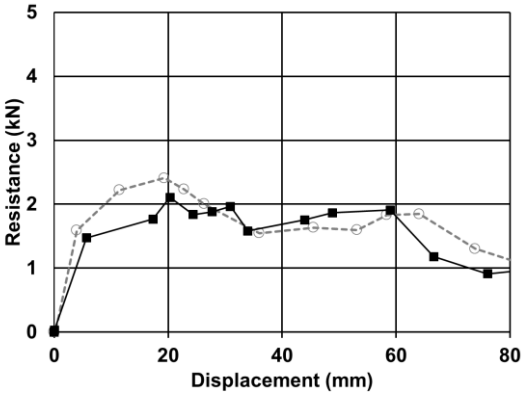

(a)

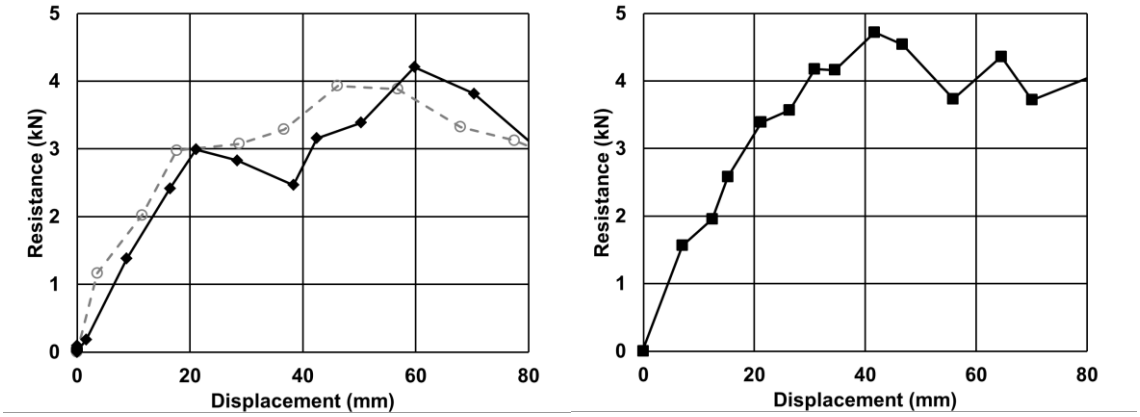

(b) (c)

Figure 7: Sleeper end resistance versus displacement plots : (a) Test E : x = 400 mm, y = 125 (b) Test F : x = 600 mm, y = 125(c) Test G : x = 800 mm, y = 125 (dimensions and loads as at full scale)

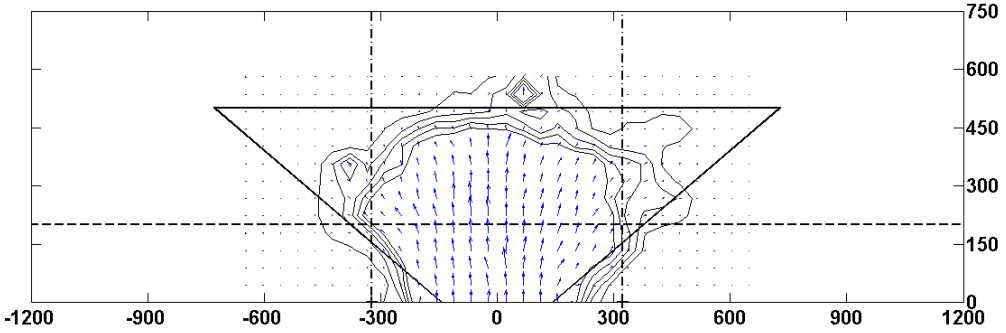

Figure 8: Deformation mechanism for the shoulder width (*x*) of 200 mm (Test A) identified from image analysis (Sleeper displacement = 10.8 mm and axes in mm).

)

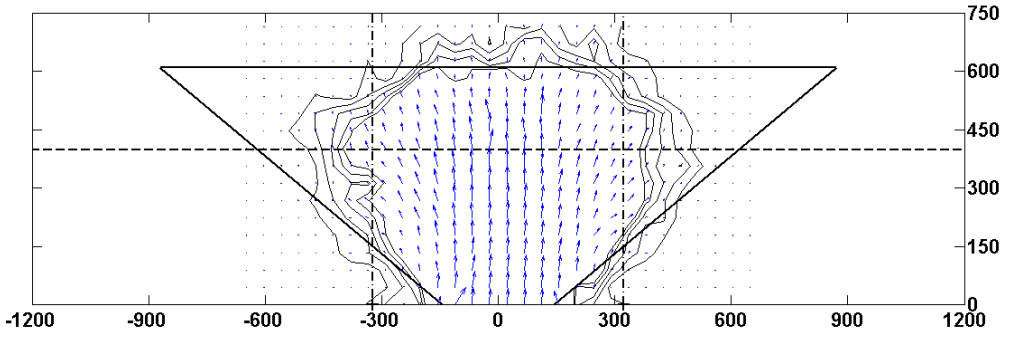

489

490 **Figure 9: Deformation mechanism for the shoulder width (x) of 400 mm (Test B) identified from image**
491 **analysis (Sleeper displacement = 27.0 mm and axes in mm).**

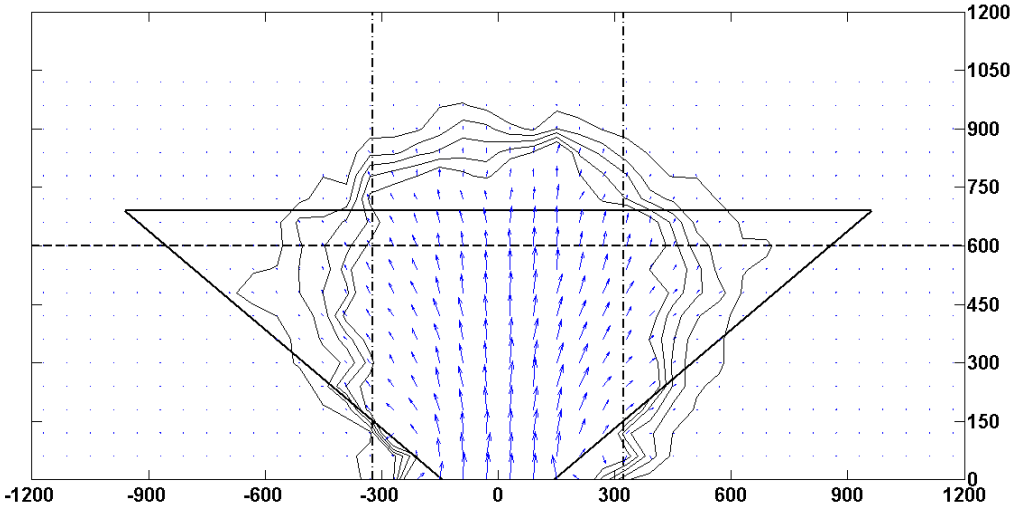

492

493 **Figure 10: Deformation mechanism for the shoulder width (*x*) of 600 mm (Test C) identified from image**
494 **analysis (Sleeper displacement = 36.0 mm and axes in mm)**

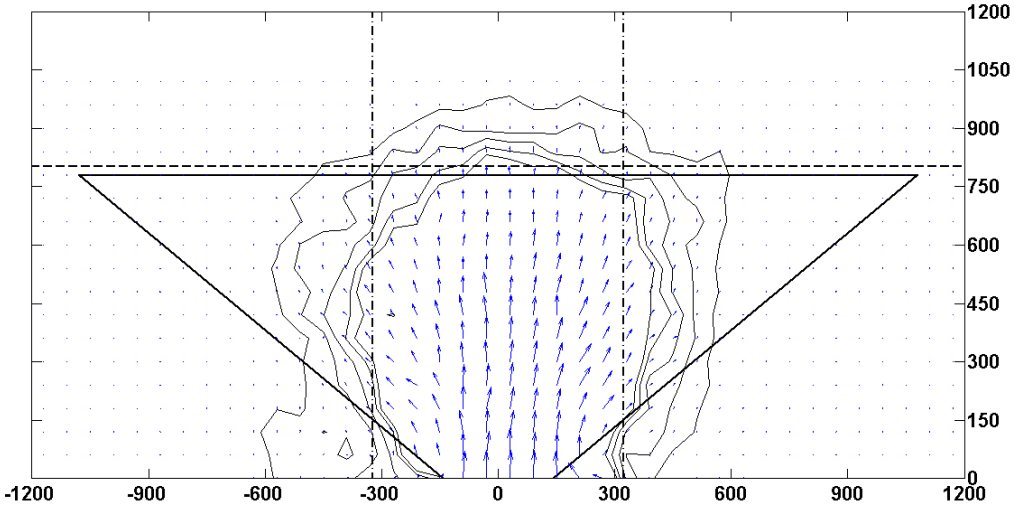

495

496 **Figure 11: Deformation mechanism for the shoulder width of 800 mm (Test D) identified from image**
497 **analysis (Sleeper displacement = 38.4 mm and axes in mm)**

498

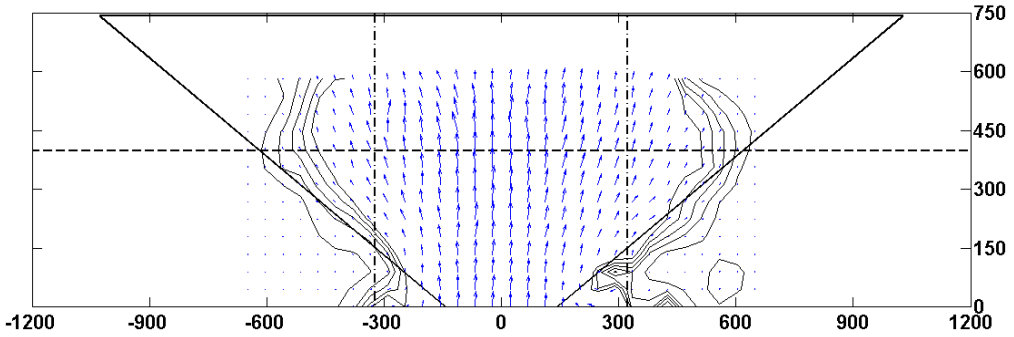

499

500 **Figure 12: Deformation mechanism for the shoulder width (*x*) of 400 mm and heap of 125 mm (*y*) (Test**
501 **E) identified from image analysis (Sleeper displacement = 18 mm and axes in mm)**

502

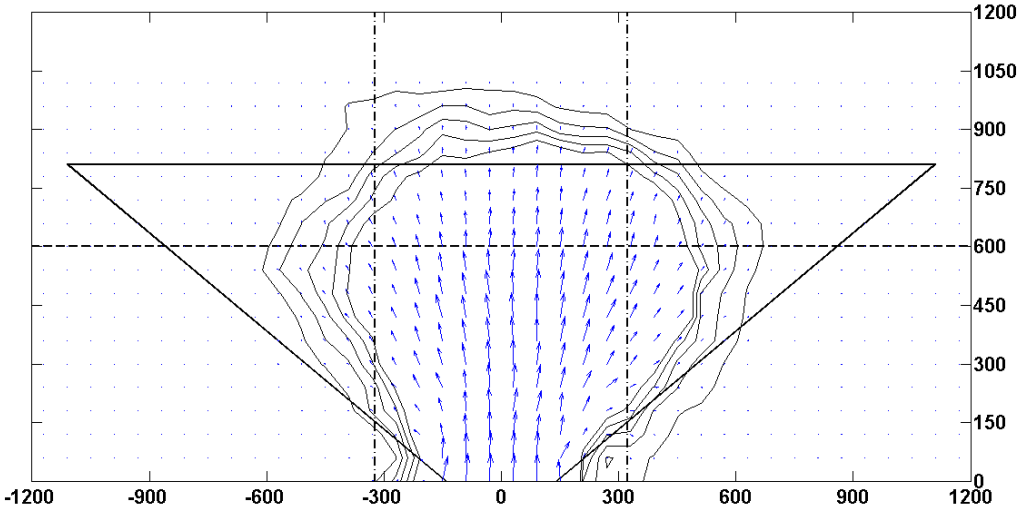

503

504 **Figure 13: Deformation mechanism for the shoulder width (*x*) of 600 mm and heap of 125 mm (*y*) (Test**
505 **F) identified from image analysis (Sleeper displacement = 45 mm and axes in mm)**

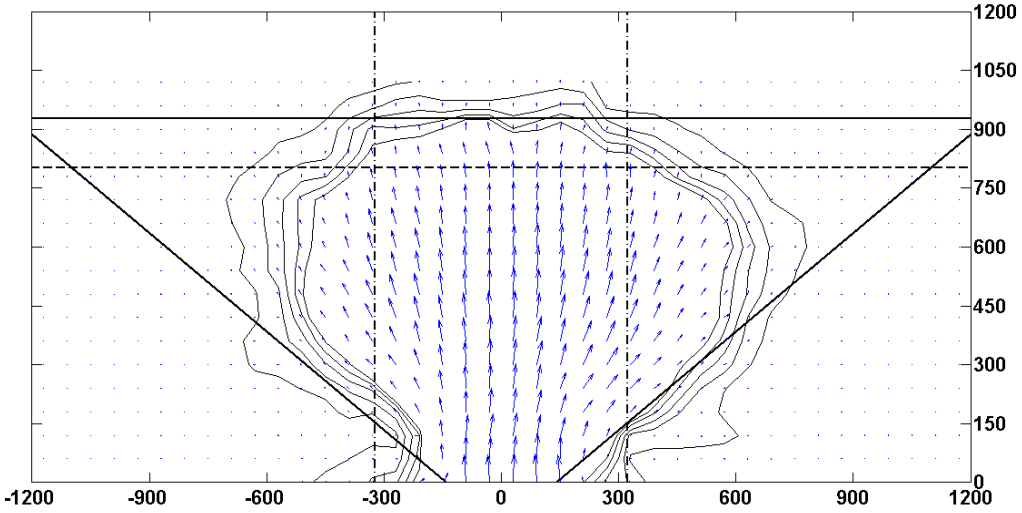

506

507 **Figure 14: Deformation mechanism for the shoulder width (*x*) of 800 mm and heap of 125 mm (*y*) (Test**
508 **G) identified from image analysis (Sleeper displacement = 45 mm and axes in mm)**

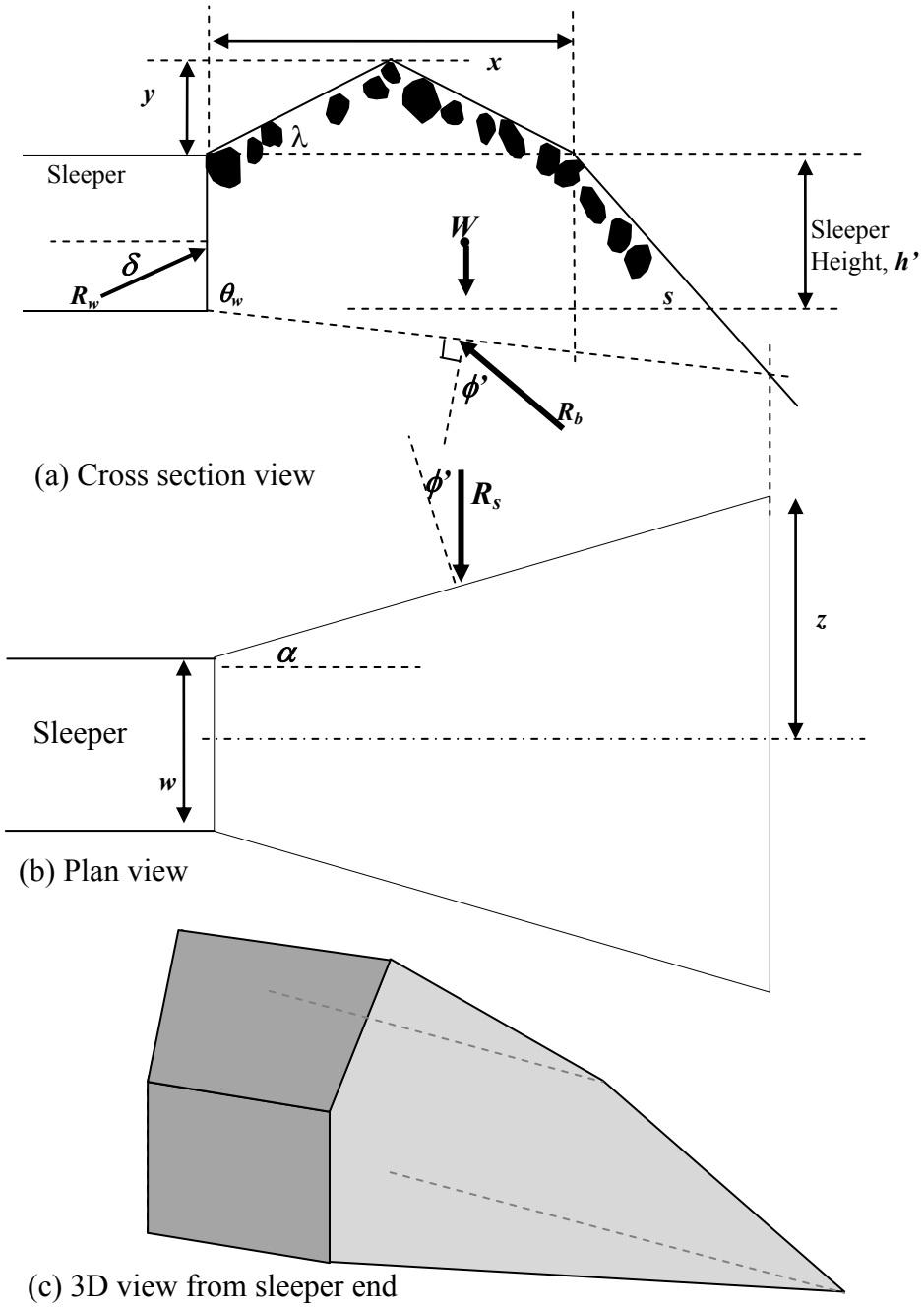

509

510 **Figure 15: Potential failure mechanism for shoulder ballast as sleeper end is pushed into ballast**

511

512

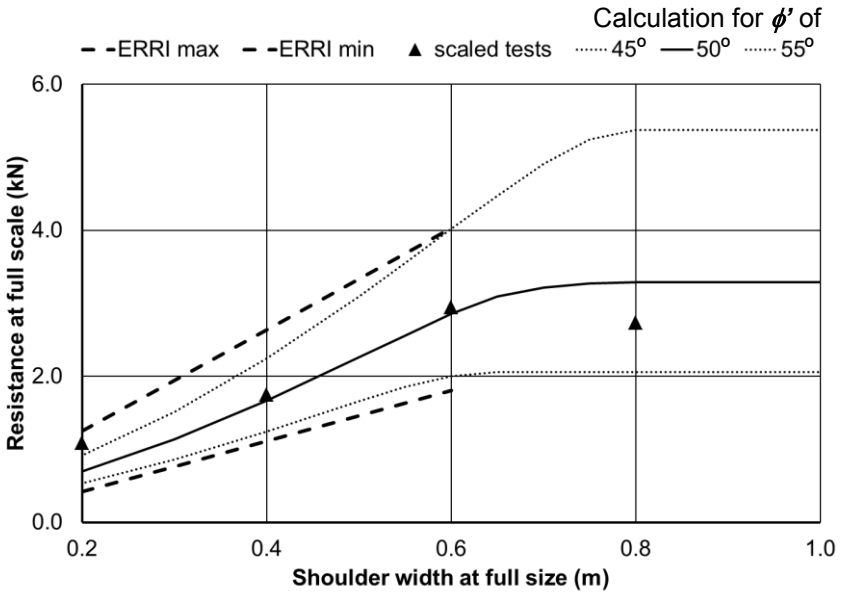

513

514 **Figure 16: Shoulder resistance against shoulder width, for level ballast shoulders (test results average for**
515 **same size of shoulder)**

516

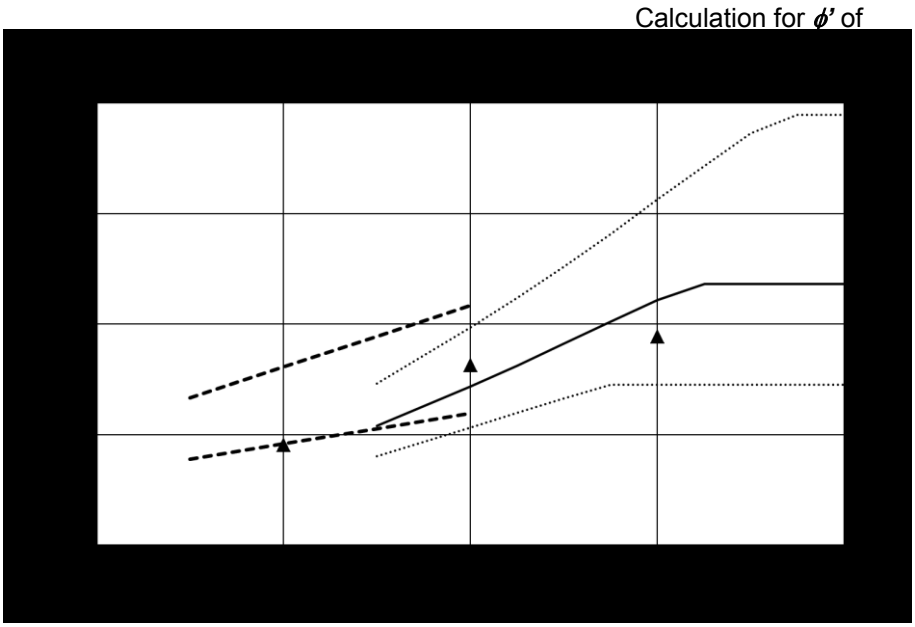

517

518 **Figure 17: Shoulder resistance against shoulder width, for 125 mm heaped shoulders (test results average**
519 **for same size of shoulder)**

520

521

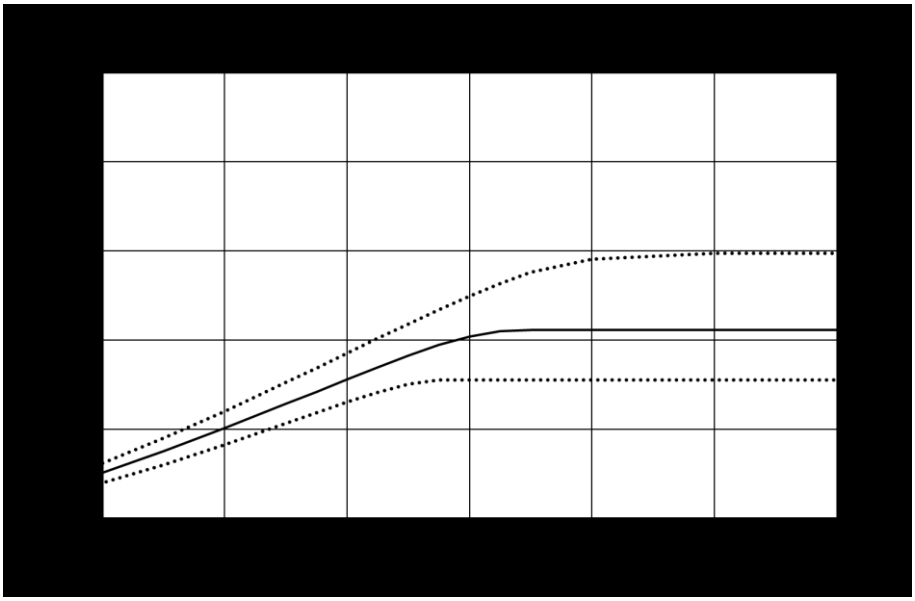

Figure 18: Shoulder resistance against shoulder width, per sleeper for 0.65 m sleeper spacing and level ballast shoulders

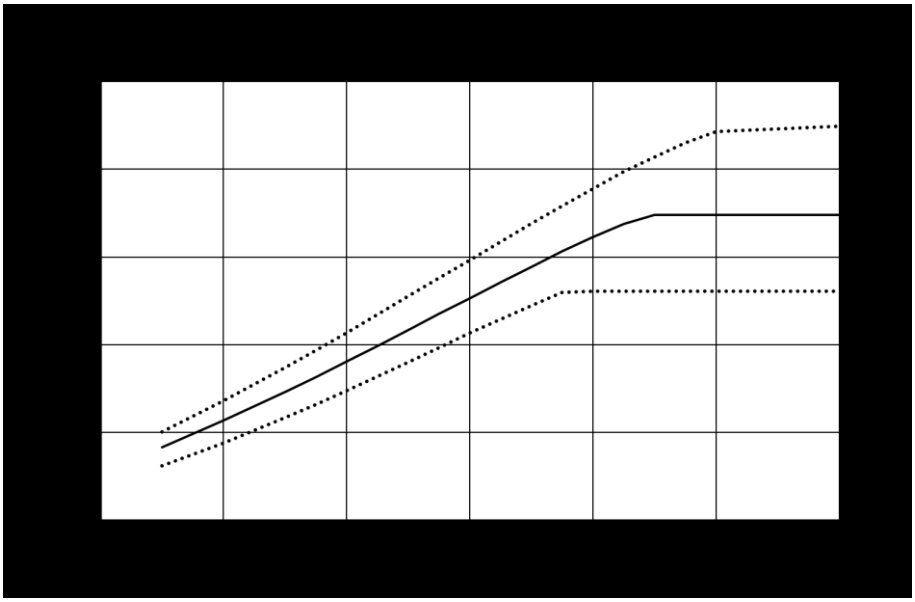

Figure 19: Shoulder resistance against shoulder width, per sleeper for 0.65 m sleeper spacing and 125 mm heaped ballast shoulders

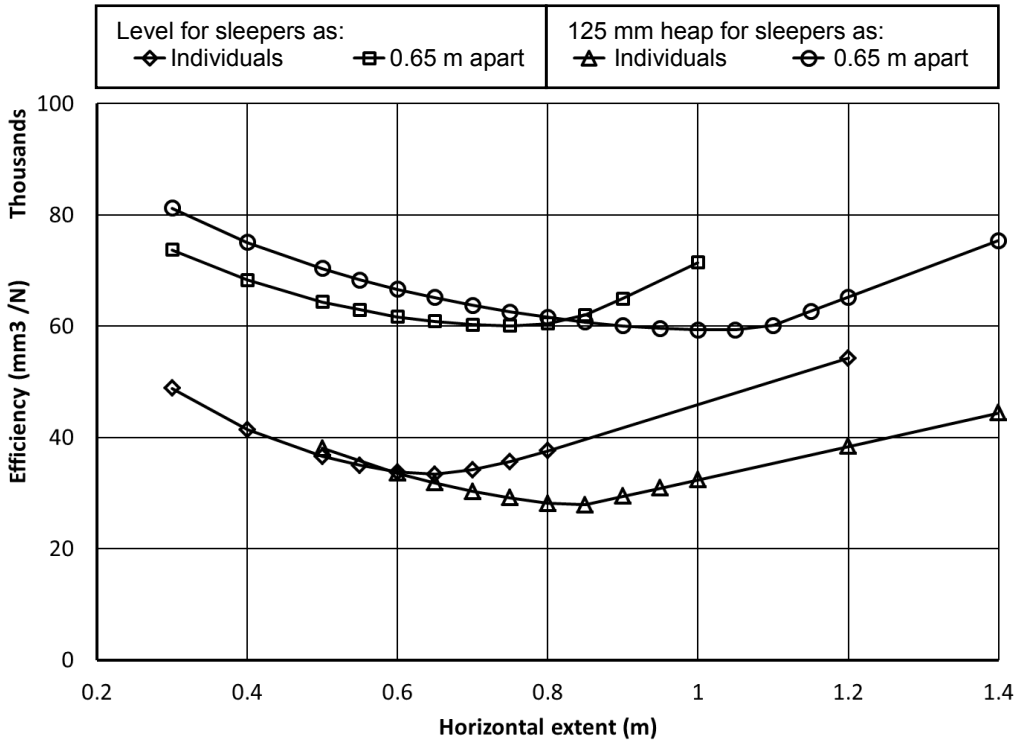

529

530 **Figure 20: Calculated efficiency of shoulder for 50º effective angle of shearing resistance for individual**
531 **sleeper ends and per sleeper for 0.65 m spacing**

532

533

534 TABLES

Initial dry density (kg/m^3)	Initial Confining stress σ_3' (kPa)	Axial stress σ_1' at ϕ_{peak} (kPa)	ϕ_{peak} (corrected)
1555	15.9	117.9	47.4
1558	26	177.5	47.1
1549	31.3	214.8	46.4
1537	37	261.0	47.7
1580	58.9	408.4	48.1
1570	116.7	757.5	46.6
1567	200.3	1120.2	43.6
1583	300.5	1500.6	41.5

535 Table 1: Key data from representative triaxial monotonic failure tests on scaled ballast

536

Source	Rock type/tested saturated or dry/sample size (diameter × height in mm)/ membrane	ρ_d (kg/m^3)	σ_3' (kPa)	q'$_{peak}$ (kPa)	ϕ'_{peak} (º)
Anderson and Fair (2008)	Granite/Dry/236×455/ 2×0.75 mm thick rubber	1450	40	308	52.5
		1470	90	544	48.7
		1470	140	631	43.8
Aursudkij et al., (2009)	Limestone/Dry/300×450 Two 2 mm and 1 mm thick latex	1511	10	96	55.9
		1539	30	242	53
		1545	60	375	49.3
Indraratna et al., (1998)	Latite basalt/Saturated/300×600 4mm thick rubber	1530	15	320	64.4
		1530	30	390	61.1
		1530	60	640	55.9
		1530	90	730	53.3
		1530	120	840	51.5
		1530	240	1275	46.7
Raymond and Davies (1978) - loose	Dolomite/Saturated/225×450 Not stated	1400	17	-	44.1
		1400	35	-	40
		1400	51	-	37.6
		1400	103	-	39.8
		1400	206	-	37
		1400	310	-	37
Raymond and Davies (1978) - dense	Dolomite/Saturated/225×450 Not stated	1700	17	190	56
		1700	35	280	52.5
		1700	51	320	48.1
		1700	103	570	45.9
		1700	206	1015	44.1
		1700	310	1400	42.9
Suiker et al., (2005)	Basalt/Dry/254×645/ 0.76 mm thick latex	1610	10.3	75	51.7
		1700	41.3	275	49.5
		1620	68.9	387	47.5

537 Table 2: Key features of triaxial tests taken from literature, data either taken directly or inferred from graphs

538

539

Test	Full scale shoulder (Fig. 1)		1/3 scale shoulder		Borders of testing area (Fig. 5) (mm)
	Width ***x*** (mm)	Height ***y*** (mm)	1/3 width ***x*** (mm)	1/3 height ***y*** (mm)	
A	200	0	67	0	500
B	400	0	133	0	500
C	600	0	200	0	1000
D	800	0	267	0	1000
E	400	125	133	42	500
F	600	125	200	42	1000
G	800	125	267	42	1000

540 Table 3: Geometrical details of scaled ballast tests

541

Test	Number of tests	Characteristic average peak data from scaled tests mapped to full size	
		Characteristic Peak (kN)	Sleeper Deflection
A	3	1.1	20
B	2	1.7	25
C	2	2.9	35
D	3	2.7	35
E	2	2.3	20
F	2	4.1	50
G	1	4.7	50

542 Table 4: Peak shoulder resistance and corresponding deflections from scaled tests, reported as for full size
543 sleepers and ballast
544

545

Parameter	Symbol	Value	Source or notes
sleeper height	h	0.21 m	Manufacturer's data (Tarmac G44)
sleeper width	w	0.29 m	0.29 m at the base (G44 sleeper)
sleeper spacing	s	0.65 m	Typical UK spacing
Density of ballast	ρ_b	1,500 kg/m^3	Estimated as placed density in tests
Width of shoulder	x	Varied	RSSB. (2003)
Height of top	y	0 to 0.125 m	
Angle friction ballast/sleeper	δ	0° to 24°	Permitted to mobilise equal to 0.5×(90-θ)until it reaches its maximum value of ~24° found from tests of base ballast L/V ratio (Le Pen and Powrie 2011)
Angle of wedge for shoulder	θ_w	Varied	adjusted to give minimum resistance
Angle of heap	λ	Varied	Set for each calculation to match the initial geometry
angle of effective shearing resistance	ϕ'	45° to 55°	Based on triaxial test data
Slope angle	s	45°	Measured as the approximate angle of repose

546 Table 5: Parameter values used in limit equilibrium calculation of shoulder resistance

547

548

Shoulder size: (x) × (y)	Soil angle of effective shear strength								
	45º			50º			55º		
	θ_w	x_f	z_f	θ_w	x_f	z_f	θ_w	x_f	z_f
200×0	100º	498	640	100º	498	736	100º	498	853
400×0	90º	610	573	90º	610	869	95º	668	1097
600×0	75º	639	781	80º	689	963	85º	745	1206
800×0	70º	576	719	75º	784	1077	75º	784	1262
400×125	100º	741	882	100º	741	1026	100º	741	1200
600×125	90º	810	954	90º	810	1110	95º	888	1410
800×125	70º	681	966	85º	927	1248	90º	1011	1584

549 Table 6: Position of wedge daylight from limit equilibrium calculation